

# Car MAX-DOAS measurements around entire cities: quantification of NO<sub>x</sub> emissions from the cities of Mannheim and Ludwigshafen (Germany)

O. Ibrahim<sup>1</sup>, R. Shaiganfar<sup>1</sup>, R. Sinreich<sup>2,\*</sup>, T. Stein<sup>2,\*\*</sup>, U. Platt<sup>2</sup>, and T. Wagner<sup>1</sup>

<sup>1</sup>Max-Planck-Institute for Chemistry, Mainz, Germany

<sup>2</sup>Institute for Environmental Physics, University of Heidelberg, Heidelberg, Germany

\* now at: University of Colorado at Boulder, Boulder, USA

\*\* now at: Ernst & Young, 7, Parc d'Activit Syrdall, Munsbach, Luxembourg

Received: 2 February 2010 – Published in Atmos. Meas. Tech. Discuss.: 11 February 2010

Revised: 4 May 2010 – Accepted: 3 June 2010 – Published: 22 June 2010

**Abstract.** We present car Multi-Axis (MAX-) DOAS observations of tropospheric NO<sub>2</sub> carried out on circles around the cities of Mannheim and Ludwigshafen (Germany) on 24 August 2006. Together with information on wind speed and direction, the total emissions of the encircled source(s) are quantified from these measurements. In contrast to recent similar studies based on zenith scattered sun light (elevation angle of 90°), we use a MAX-DOAS instrument mounted on a car, which observes scattered sun light under different elevation angles (here 45°, and 90°). Compared to simple zenith sky observations, MAX-DOAS observations have higher sensitivity and reduced uncertainty, and avoid systematic offsets in the determination of the vertically integrated trace gas concentration. The determination of the absolute value of the integrated tropospheric trace gas concentrations is especially important for the calculation of absolute trace gas fluxes through arbitrary transects. However, even if emission sources are completely surrounded, systematic offsets in the measured vertically integrated trace gas concentration can lead to errors in the determined total emissions, especially for observations around extended areas. In this study we discuss and quantify different error sources. In most cases, the largest error source is the variability and imperfect knowledge of the wind field. In addition – depending on the trace species observed – also chemical transformations between the emission sources and the measurement location have to be considered. For that purpose we use local observations within the encircled area to quantify and/or correct these errors. From our observations we derive a total NO<sub>x</sub> emission from the Mannheim/Ludwigshafen

area of  $(7.4 \pm 1.8) \times 10^{24}$  molec/sec, which if assumed to be constant throughout the year would correspond to a total emission of  $17\,830 \pm 4340$  t/yr (calculated with the mass of NO<sub>2</sub>) t/yr, consistent with existing emission estimates. From our observations it is also possible to separately determine the average influx into the Mannheim/Ludwigshafen area ( $5.4 \pm 0.9 \times 10^{24}$  molec/sec or  $13\,010 \pm 2170$  t/yr) and the average outflux ( $12.8 \pm 1.8 \times 10^{24}$  molec/sec or  $13\,010 \pm 4340$  t/yr).

## 1 Introduction

The precise knowledge of the emissions of natural and anthropogenic trace gases (e.g. pollutants or greenhouse gases) is important for many applications. Emission estimates are used as input to atmospheric chemistry and transport models. By varying the strengths of the emission sources in the model, it is e.g. possible to predict which emission reductions would have the strongest impact on air quality in a given area. Similar arguments hold for the emission inventories of greenhouse gases, which are important input in models predicting future climate. Accurate knowledge of the emission strengths from different sources is especially important to quantify the influence of anthropogenic emissions in comparison to natural emissions.

Usually, emission inventories are built using bottom-up strategies. Emission strengths of individual sources are quantified and summed up according to the frequency of the respective source type. Uncertainties of the calculated emission inventories result from both errors in the estimate of the number of individual sources and errors in the emission strength of individual sources.



Correspondence to: T. Wagner  
(thomas.wagner@mpch-mainz.mpg.de)

An alternative to bottom-up emission inventories are top-down emission inventories. They are based on measurements of the atmospheric concentration of a pollutant, which is then related to the emission strength of an individual source or an integrated source strength within a specified area. For the determination of the emission strength of an observed trace gas additional knowledge on the atmospheric transformation processes (transport and chemistry) is required. Depending on the complexity of the emission source (e.g. a point source or a mixture of different sources with different spatio-temporal emission patterns) and the information content of the measurement (e.g. point measurements at fixed locations, or satellite observations), either simple assumptions (e.g. on the atmospheric lifetime and wind fields), or complex inverse models are required.

In this study we estimate the total urban  $\text{NO}_x$  emissions from car MAX-DOAS observations performed on circular driving routes around complete cities. This method was recently introduced and applied to determine emissions of  $\text{SO}_2$ ,  $\text{NO}_2$  and  $\text{HCHO}$  (Johansson et al., 2008; Johansson et al., 2009; Rivera et al., 2009). In contrast to these zenith sky observations we use MAX-DOAS observations, which have several advantages: first because of the slant path through the troposphere they have a higher sensitivity for tropospheric trace gases. While this effect is not very important for the rather high elevation angle used in this study, the sensitivity is largely increased for smaller elevation angles (by about a factor of three for elevation angles around  $20^\circ$ ).

Second, the uncertainty of the absorption path length is in general smaller compared to zenith sky observations. Moreover, MAX-DOAS observations are less affected by light path modifications caused by multiple scattering in thick clouds (see e.g. Johansson et al. (2008)), because the measurements at different elevation angles are affected by such clouds in a similar way. Third, MAX-DOAS observations allow to determine the vertically integrated tropospheric trace gas concentration (vertical column density, VCD) above the instrument location without systematic biases (Wagner et al., 2010). In contrast, from zenith looking instruments only the difference of the tropospheric VCD compared to a reference measurement can be determined.

This complicates the interpretation of the measurements especially in cases when emission sources are not completely encircled (Johansson et al., 2009). However, even if emission sources are completely surrounded, systematic offsets in the measured vertically integrated trace gas concentration can lead to errors in the determined total emissions: for example if changing wind direction and speed have to be considered (e.g. wind speed is different for the influx region compared to the outflux region), it is essential that the absolute tropospheric VCDs are used for the flux calculations. A similar problem is related to the effects of chemical transformations (e.g. chemical destruction or deposition). Since the rate of chemical destruction depends (besides other dependencies) on the absolute trace gas concentration, the knowledge on the

## 2-dimensional integration of the tropospheric trace gas concentration

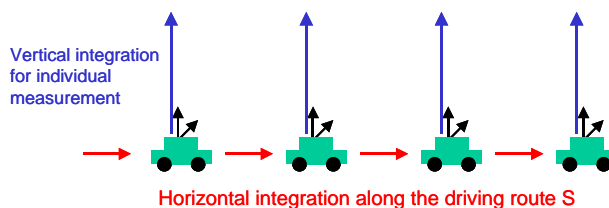


**Fig. 1.** From MAX-DOAS observations the vertically integrated tropospheric trace gas concentrations can be determined. If MAX-DOAS observations are performed on mobile platforms, a second integration along the driving route becomes possible (indicated by the blue arrows). The black arrows indicate the viewing directions of the MAX-DOAS instrument.

absolute tropospheric VCDs in the influx and outflux regions is essential for their correct quantification. Both aspects become especially important for observations around extended areas.

The determination of absolute tropospheric VCDs from MAX-DOAS observations is also important for the quantitative comparison with model results and for the validation of satellite observations.

In addition to the inherent vertical integration of the tropospheric trace gas concentration by MAX-DOAS observations, a horizontal integration can be carried out if MAX-DOAS observations are performed from aircrafts or cars. Such observations eventually allow to determine the complete flux  $F$  of trace gas molecules across the area span by the driving route  $S$  and the vertical (see Fig. 1). For that purpose the knowledge of the wind speed and direction is required:

$$F = \int_S \text{VCD}(s) \cdot \vec{W} \cdot \vec{n}(s) \cdot ds \quad (1)$$

Here  $\vec{n}(s)$  indicates the normal vector parallel to the Earth's surface and orthogonal to the driving direction at the position  $s$  of the driving route;  $\vec{W}$  is the average wind vector within the trace gas layer. We carry out Car MAX-DOAS measurements along closed driving routes around large emissions sources, e.g. whole cities (Fig. 2). If the emission sources are completely encircled, the total flux entering the encircled area (on the side from which the wind blows) as well as the total flux leaving the encircled area (at the opposite side, see Fig. 2) can be determined (see also Johansson et al., 2008). In simple cases, the difference between both fluxes yields the integrated total emission of the encircled area. To determine the total flux  $F_{\text{total}}$  of the encircled area the integral in Eq. (1) has to be evaluated along the complete circle around the area of interest:

$$F_{\text{total}} = \int_A \text{div}(\text{VCD} \cdot \vec{W}) dA = \oint_S \text{VCD}(s) \cdot \vec{W} \cdot \vec{n} \cdot ds \quad (2)$$

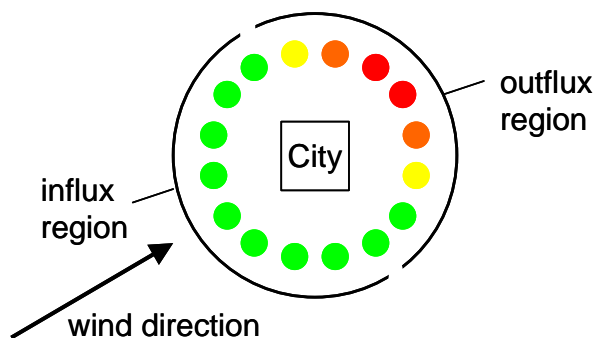


**Fig. 2.** Example of tropospheric vertical column densities (orange and red colours indicate enhanced values) derived from mobile MAX-DOAS observations around an extended emission source. According to the wind direction a part of the observations characterises air masses entering and a part of them leaving the encircled area.

It should be noted that for the complete surrounding of extended areas the driving period is typically between a few ten minutes and more than one hour. Thus temporal variations on time scales below that period can not be resolved and the resulting emission estimates are only representative for the average conditions through that period. Two main effects complicate the determination of the total emission and have to be taken into consideration:

(A) *Variation of the wind field*

In the simplest case, a wind field with constant speed and direction is present over the complete area of interest, and the wind speed is also high enough that the transport across the encircled area is fast compared to the atmospheric lifetime of the trace gas. In more complicated cases, the wind speed is low and varies with time and location within the encircle area. In such cases, emission estimates are difficult and might only be possible with the additional use of atmospheric model simulations. A further general problem is caused by the fact that the wind speed usually increases with altitude (also the direction changes systematically), but the vertical distribution of the observed trace gas is usually not well known. Thus assumptions on the vertical distribution and appropriate wind speed have to be made.

(B) *Chemical transformations*

Chemical transformations and deposition processes change the trace gas abundance after the emission process. Depending on the speed, two cases can be distinguished. First, rapid chemical reactions can change the partitioning of the emitted species. In this study, MAX-DOAS observations of  $\text{NO}_2$  are investigated, while most of the  $\text{NO}_2$  was primarily emitted as  $\text{NO}$ . The partitioning of both species depends on the ozone concentration

and the  $\text{NO}_2$  photolysis rate. In order to quantify the total  $\text{NO}_x$  ( $\text{NO}_2 + \text{NO}$ ) emissions, the so called Leighton ratio ( $L = [\text{NO}]/[\text{NO}_2]$ ) has to be known (or assumed). Second, the atmospheric concentration of the emitted species can be changed by processes, which are fast compared to the transport time between the emission source and the location of the measurement. Thus, the measured trace gas concentration represents only a fraction of the emitted trace gas abundance. These destruction processes are usually described by an exponential decrease with an e-folding lifetime  $\tau$ , after which the trace gas concentration is reduced to a fraction  $1/e$  of the initial value. It should be noted that in cases of substantial trace gas destruction between the emission source and the location of the measurement (short atmospheric lifetime compared to the transport time), also the spatial distribution of the emission sources within the encircled area becomes important.

These potential error sources are discussed in detail and quantified for the Car MAX-DOAS measurements presented in this study (see Sect. 4).

The paper is structured as follows: in Sect. 2 the MAX-DOAS method is briefly introduced and the performed Car MAX-DOAS measurements are described. Section 3 provides details on the different steps of the data analysis. In Sect. 4 the results of our measurements are presented and the uncertainties caused by the different error sources are discussed and quantified. In Sect. 5 the results of our study are summarised and detailed recommendations for future measurements are given.

## 2 MAX-DOAS observations

In recent years Multi-Axis-Differential Optical Absorption Spectroscopy (MAX-DOAS) observations have become a widely and successfully used technique for the remote sensing of tropospheric trace gases and aerosols. MAX-DOAS instruments observe scattered sun light under different slant viewing angles, which make them especially sensitive to tropospheric trace gases and aerosols (e.g. Hönninger et al., 2002; Van Roozendaal et al., 2003; Wittrock et al., 2004; Wagner et al., 2004, 2007; Brinksma et al., 2008). From MAX-DOAS observations, vertical profiles of tropospheric trace gases and aerosol extinction can be retrieved yielding up to a few pieces of information, with the highest vertical resolution close to the surface (see e.g. Theys et al., 2007). However, profile retrievals are typically restricted to MAX-DOAS measurements made at fixed locations and under cloud free conditions. For MAX-DOAS observations made from moving platforms, horizontal gradients of the trace gas concentration often prevent a meaningful profile retrieval. In addition, unlike ship measurements, for car measurements the observations at low elevation angles are usually affected

by obstacles (e.g. trees or houses) in the field of view. Thus from mobile MAX-DOAS observations usually only the (absolute) tropospheric VCD is determined.

## 2.1 Determination of the tropospheric VCD

For the retrieval of the tropospheric VCD, typically observations at rather high elevation angles (>about 10°) are used. For such elevation angles the effects of atmospheric aerosols are rather small and the atmospheric light paths can be geometrically well approximated (Brinkma et al., 2008; A. Richter, personal communication, 2005). In addition, the retrieval of tropospheric VCDs is usually even possible in the presence of clouds (at least for trace gases located below the cloud base).

For the analysis of MAX-DOAS observations it is usually assumed that the concentration field does not change during the time period needed for the observations at the different elevation angles. This assumption is roughly valid for MAX-DOAS observations made at fixed locations. In contrast, mobile MAX-DOAS observations are typically strongly affected by horizontal concentration gradients of air masses probed along the driving route. For these platforms, the usual way of the MAX-DOAS data analysis can thus lead to large errors, in extreme cases even negative concentrations might be obtained. Recently a technique was developed which overcomes this problem and allows to determine absolute tropospheric VCDs along the driving route (Wagner et al., 2010).

## 2.2 Car MAX-DOAS instrumentation for the Mannheim/Ludwigshafen measurements

The Mini-MAX-DOAS instrument is a fully automated, light-weight spectrometer (13 cm·19 cm·14 cm) designed for the spectral analysis of scattered sunlight (e.g. Bobrowski et al., 2003). It consists of a sealed aluminium box containing the entrance optics, a fibre coupled spectrograph and the controlling electronics. A stepper motor mounted outside the box rotates the whole instrument to control the elevation of the viewing angle (angle between the horizontal and the viewing direction). The entrance optics consists of a quartz lens of focal length  $f=40$  mm coupled to a quartz fibre bundle which leads the collected light into the spectrograph (field of view is  $\sim 1.2^\circ$ ). The light is dispersed by a crossed Czerny-Turner spectrometer (USB2000, Ocean Optics Inc.) with a spectral resolution of 0.7 nm over a spectral range from 320–460 nm. A one-dimensional CCD (Sony ILX511, 2048 individual pixels) is used as detector. Before the signal is transferred to the 12 bit analog-to-digital converter, an electronic offset is added. After conversion, the signal is digitally transmitted to a laptop computer via a USB cable and stored for subsequent analysis.

For the mobile measurements the Mini-MAX-DOAS instrument was mounted on the top of a car with the telescope pointing in driving direction and was powered by the 12V car battery. The rest of the set-up was inside the car and both parts were connected via two electric cables. The measurements are controlled from a laptop using the DOASIS software (Kraus, 2004).

On 24 August 2006, measurements were carried out around the Mannheim-Ludwigshafen industrial/urban area. The sequence of elevation angles was chosen to: 45°, 45°, 45°, 45°, 90°, and the duration of an individual measurement was about 20–25 s. The position of the individual measurements was determined from the measurement time. The relationship between time and location was established by assigning the exact times while passing the distance signs on the motorway. To simplify the measurements, in future applications position data using GPS observations (as e.g. used by Johansson et al., 2008), should be used.

## 3 Data analysis

The measured spectra are analysed using the DOAS method (Platt and Stutz, 2008). A wavelength range of 415–435 nm was selected for the analysis. Several trace gas absorption cross sections ( $\text{NO}_2$  at 297 K (Vandaele et al., 1998),  $\text{H}_2\text{O}$  at 300 K (Rothmann et al., 2005),  $\text{O}_4$  at 296 K (Greenblatt et al., 1990), and  $\text{O}_3$  at 243 K, Bogumil et al., 2003) as well as a Fraunhofer reference spectrum, a Ring spectrum (calculated from the Fraunhofer spectrum) and a polynomial of second order were included in the spectral fitting process (using the WinDOAS software (Fayt and van Roozendaal, 2001)). The wavelength calibration was performed based on a high resolution solar spectrum (Kurucz et al., 1984). The output of the spectral analysis is the slant column density (SCD), the integrated trace gas concentration along the light path through the atmosphere. Following to the retrieval technique of Wagner et al. (2010) the tropospheric  $\text{NO}_2$  VCD is determined from each observation made at 45° elevation angle using the zenith measurement of the respective sequence. In the retrieval process, tropospheric air mass factors (AMF) are needed, for which the geometric approximation is used (here  $\alpha$  is the elevation angle of the telescope):

$$\text{AMF}(\alpha) = 1/\sin(\alpha) \quad (3)$$

Depending on the aerosol load and on the vertical distribution of the trace gas, the geometrical approximation for the tropospheric AMF can deviate to some degree from the true value. We investigated these deviations using the Monte Carlo radiative transfer model TRACY-2 (Wagner et al., 2007; Deutschmann and Wagner, 2008). The errors of the geometric approximation depend on the SZA and relative azimuth angle (in general they increase with increasing SZA and relative azimuth angle). For aerosol loads with optical depth  $<0.5$  and for surface-near trace gases ( $<200$  m)

the errors of the geometrical approximation are typically below 15%. It is interesting to note here that for MAX-DOAS observations the uncertainties of the tropospheric AMF are usually smaller than for the observation of zenith scattered light. This aspect is not of great importance for this study, because of the rather high elevation angle of 45° (leading to a reduction of the uncertainty by 10–30%). However, for elevation angles around 20° (see e.g. Wagner et al. (2010)) it typically results in a reduction of the uncertainties by about 50% (elevation angles <20° might not be very useful for car MAX-DOAS observations, because of trees and buildings in the field of view). In the presence of clouds the uncertainties can in principle become larger. However, especially for the part of the trace gas profile below the cloud (e.g. freshly emitted NO<sub>x</sub>) the geometrical approximation is in general a very good choice, because the lower boundary of the cloud acts as well defined illumination source and scattering events below the cloud (within the trace gas layer) become less important.

The total error of the tropospheric NO<sub>2</sub> VCD is estimated from the typical fit residual and the uncertainty of the geometric approximation to <3×10<sup>15</sup> molec/cm<sup>2</sup> or <15%.

## 4 Results and discussion

Results of the car MAX-DOAS observations made on trips around the cities of Ludwigshafen and Mannheim (Southern Germany, see Fig. 3) on 24 August 2006 are shown in Figs. 4 and 5. The sky was mainly overcast and temperatures were around 20°C. Both cities were surrounded in four successive “circles” with approximate extensions of 26 km in north-south direction and 18 km in east-west direction. During these circles, a repeating pattern with high and low tropospheric NO<sub>2</sub> VCDs was found. In general the highest NO<sub>2</sub> VCDs were measured in the north-east corner, which can be directly related to the prevailing wind direction on that day (mainly from south-west). However, not exactly the same patterns are obtained for the different circles reflecting the variation of emissions as well as wind speed and direction.

From the MAX-DOAS observations the integrated NO<sub>x</sub> emission within the encircled area can in principle be calculated according to Eq. (2). However, to account for the finite atmospheric lifetime and for the partitioning between NO and NO<sub>2</sub>, two corrections have to be applied to Eq. (2):

$$F_{\text{NO}_x} = c_L \cdot c_\tau \cdot F_{\text{NO}_2} = c_L \cdot c_\tau \cdot \oint_S \text{VCD}_{\text{NO}_2}(s) \cdot \vec{W} \cdot ds \quad (4)$$

Here  $c_L$  is a correction factor which accounts for the partitioning of NO<sub>x</sub> into NO and NO<sub>2</sub>, which is a function of the Leighton ratio ( $L=[\text{NO}]/[\text{NO}_2]$ );  $c_L=1+L$ .  $c_\tau$  is a correction factor which accounts for the destruction of NO<sub>x</sub> while it is transported from the emission sources to the locations of the measurements.

**Table 1.** Wind data calculated from three stations (Mannheim center, south, north, see Fig. 5). For each cycle, the average and standard deviation of wind speed and direction are calculated.

| Circle | time              | Wind direction (°)<br>(wind from north is zero) | Wind speed<br>(cm/s) |
|--------|-------------------|---|----------------------|
| 1      | 1, 10:30–12:00    | 239 (±44)                                       | 268±109              |
| 2      | 2, 11:30 – 13:00  | 265 (±17)                                       | 226±101              |
| 3*     | 3*, 13:00 – 14:30 | 223 (±18)                                       | 267±71               |
| 4      | 4, 13:30 – 15:00  | 219 (±14)                                       | 314±85               |

\*L3 partly overlaps with L4, see Fig. 4

In the following sub-sections the three factors of Eq. (4) are determined separately and applied to the measurements on 24 August 2006.

### 4.1 Integration of the tropospheric NO<sub>2</sub> flux along the driving route

In this section the integral of Eq. (4) is evaluated for the MAX-DOAS measurements around the cities of Mannheim and Ludwigshafen. Because of the finite integration time of the individual spectra, the integral is substituted by a sum which is evaluated for all observations made at 45° elevation during the individual circles:

$$\begin{aligned} F_{\text{NO}_2} &= \sum_i \text{VCD}_{\text{NO}_2}(s_i) \cdot \vec{W} \cdot \vec{n} \cdot \Delta s_i \\ &= \sum_i \text{VCD}_{\text{NO}_2}(s_i) \cdot W \cdot \sin(\beta)(s_i) \cdot \Delta s_i \end{aligned} \quad (5)$$

The distance between two measurements  $\Delta s_i$  is the geometric difference between the locations at the beginning of two successive measurements. For the wind direction and wind speed  $W$  constant values for all measurements during an individual circle were assumed (for details see Sect. 4.1.1). They were calculated from half hour averages at three meteorological stations within the encircled area: Mannheim south, Mannheim center, Mannheim north (<http://mnz.lubw.baden-wuerttemberg.de/messwerte/aktuell/>), the locations are indicated in Fig. 5). Also the angles  $\beta(s_i)$  between the driving route and the wind direction were calculated in discrete steps (the angle of the driving route was determined according to the starting points of two successive spectra). The average wind speeds and directions are listed in Table 1.

As an example, Fig. 6 shows the individual terms of the sum in Eq. (5) for the fourth circle on 24 August 2006. In the top panel the tropospheric NO<sub>2</sub> VCD is shown. The second panel shows the length of the driving route for the individual measurements (the difference of the instrument position between the start of two consecutive spectra). The path length varies with the driving speed. In addition, according to the sequence of elevation angles systematically different path lengths between successive measurements are also



**Fig. 3.** The red rectangle indicates the location of the encircled area around the cities of Mannheim and Ludwigshafen in Southern Germany (see also Fig. 5). (the map was taken from <http://www.freeworldmaps.net/europe/germany/political.html>).

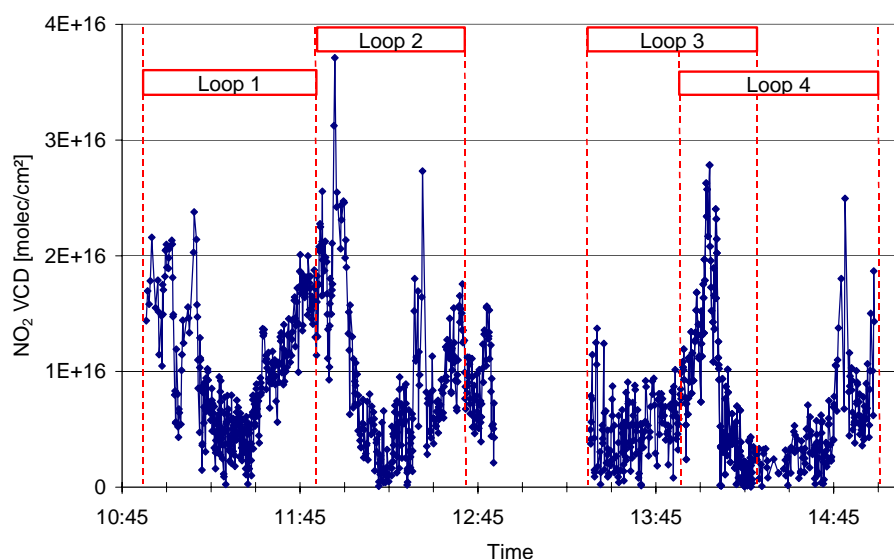


**Fig. 4.** Time series (4 circles) of the  $\text{NO}_2$  VCDs measured around Mannheim-Ludwigshafen area on 24 August 2006.

found. Larger distances occur for the end of an elevation sequence because of the gap during the record of the zenith spectrum. In addition, also some time is needed to change the elevation angle. The third panel shows the sine of the angle between the driving route and the wind direction, respectively. The bottom panel shows the resulting tropospheric  $\text{NO}_2$  flux above the driving route for the segment between two measurements taking into account also the wind speed (assumed to be constant, see Table 1). According to the relative orientation of the driving direction and wind direction, the  $\text{NO}_2$  flux is either positive or negative. The high positive

values at the beginning of the circle indicate the main emissions from the Mannheim/Ludwigshafen area. At the end of the circle both substantial negative and positive fluxes occur. They are probably caused by emissions from the city of Speyer south of the encircled area. They first enter and then leave the encircled area at the south-east edge (see Fig. 5). Besides this example, the influx (negative flux) of  $\text{NO}_2$  into the encircled area is typically rather small. Summing-up the  $\text{NO}_2$  fluxes along the driving route, yields a total emission of  $5.8 \times 10^{24}$  molecules/s  $\text{NO}_2$ . In Table 2 also the results for the other cycles are shown.

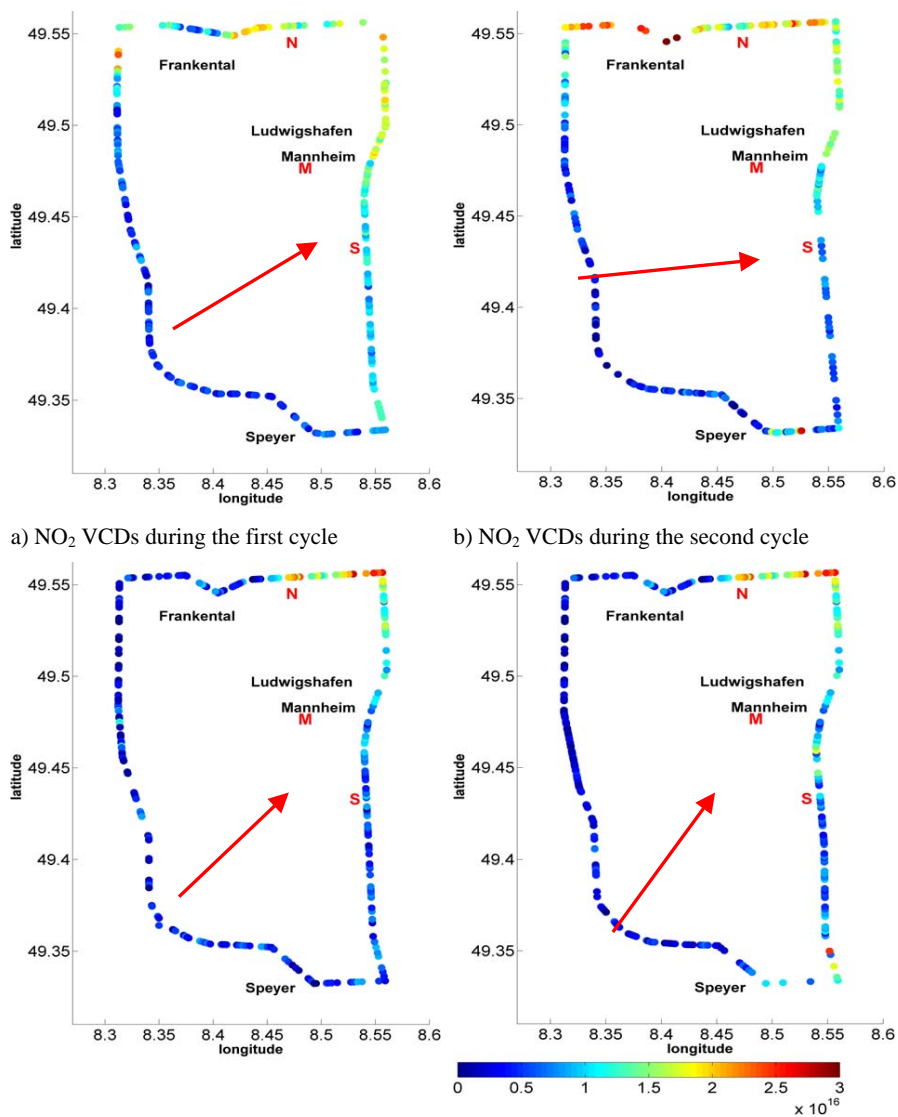


**Fig. 5.** NO<sub>2</sub> VCDs for the four individual cycles around the Mannheim-Ludwigshafen area on 24 August 2006. The letters “N”, “M”, and “S” indicate the locations of the in-situ measurement stations Mannheim North, Mannheim Center, and Mannheim South. Arrows indicate the average wind direction.

**Table 2.** Total NO<sub>2</sub> fluxes for the different circles. Also shown are the relative errors related to variations and imperfect knowledge of the wind field.

| Circle | time        | Influx<br>(molec./sec) | Outflux<br>(molec./sec) | NO <sub>2</sub> Emissions<br>(molec./sec) | Errors due to<br>wind direction | Errors due to<br>wind speed | Total error<br>due to wind |
|--------|-------------|------------------------|-------------------------|---|---------------------------------|-----------------------------|----------------------------|
| 1      | 10:30–12:00 | $-4.20 \times 10^{24}$ | $8.63 \times 10^{24}$   | $4.43 \times 10^{24}$                     | 14%                             | 21%                         | 25%                        |
| 2      | 11:30–13:00 | $-3.45 \times 10^{24}$ | $6.49 \times 10^{24}$   | $3.05 \times 10^{24}$                     | 32%                             | 23%                         | 40%                        |
| 3*     | 12:30–14:00 | $-2.83 \times 10^{24}$ | $6.89 \times 10^{24}$   | $4.05 \times 10^{24}$                     | 6%                              | 13%                         | 15%                        |
| 4      | 13:30–15:00 | $-3.46 \times 10^{24}$ | $9.26 \times 10^{24}$   | $5.80 \times 10^{24}$                     | 4%                              | 14%                         | 15%                        |

\*partly overlaps with L4

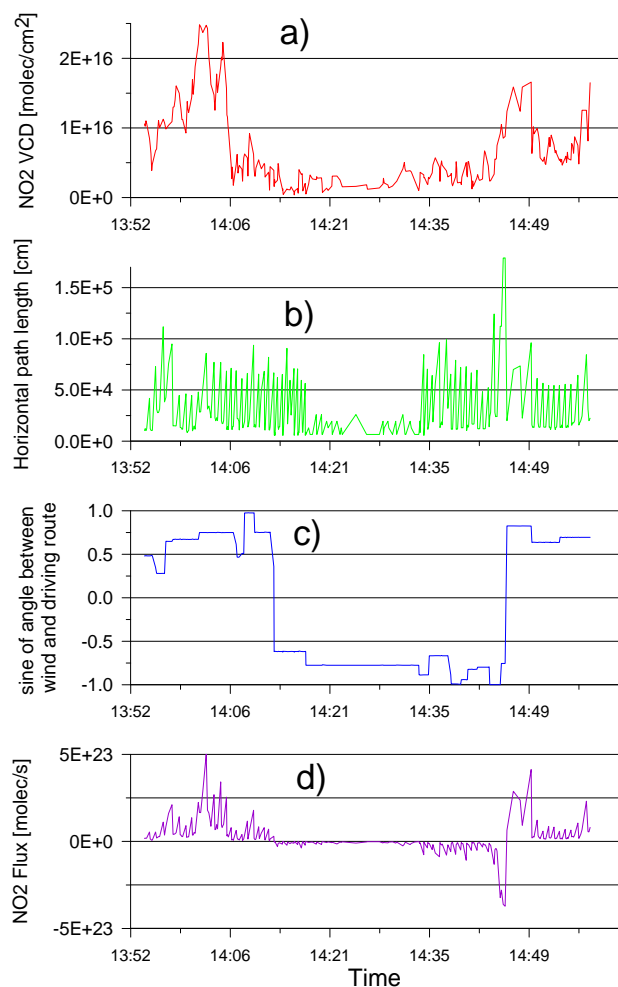


**Fig. 6.** Different components used for the net flux estimation shown for loop #4 on 24 August 2006. In (a) the observed  $\text{NO}_2$  VCD are presented. (b) shows the driving distance between two consecutive observations' and (c) the sine of the angle between the driving route and the wind direction. In d) the resulting  $\text{NO}_2$  flux is shown: negative fluxes indicate import and positive fluxes export from the encircled area.

#### 4.1.1 Errors caused by variations of the wind field

In most cases, the uncertainty of the derived total emission is dominated by the variation and the imperfect knowledge of the wind field (see also discussion in Johansson et al., 2008). In this section we discuss different possibilities to obtain wind data and to quantify the errors associated with uncertainties and variations of the wind field.

In simple cases, the variations of the wind direction and wind speed during the period of the measurements are small. In such cases (and if also the emissions are assumed to be constant with time), the determination of the emissions from the encircled area is rather simple, and average values of wind direction and wind speed can be used. Emission estimates

in previous studies (e.g. Johansson et al., 2008) are obtained using average values of the wind field, and this method is also used here (for details see below). However, in many cases, substantial temporal and spatial variations of the wind field occur, which complicate the calculation of the trace gas emissions. In such cases, also the question arises, for which locations and times the wind field should actually be considered. On the one hand it is evident that the tropospheric VCDs at the measurement location depend on the entire wind field between the location of the emission source (which is usually not precisely known) and the measurement location. On the other hand it is also obvious that for the correct consideration of the trajectory, highly resolved model data would have to be used (which should also take into account variations of the trace gas concentrations due to chemical transformations). Such model data are usually not available.

An alternative – and probably also the most adequate way – to consider wind field data for the flux calculation is to use the actual wind speed and direction at the time and location of the measurement. This procedure allows the determination of the instantaneous trace gas flux above the specific location of the measurement. Because the flux at a given location is time-dependent, such a flux calculation will only provide a snapshot, which is not necessarily representative for the average flux at that location. However, if the spatial scale of the wind fluctuations is smaller than the spatial extent of the areas of increased trace gas VCDs, the effect of the wind fluctuations will at least partially cancel out. Here it is important to note that the variations of the trace gas flux are not only caused by the fluctuations of the wind field, but also by variations of the tropospheric trace gas VCD, and the effect of variations of the wind field will partly be compensated by variations of the trace gas concentration. Besides pure statistical effects, such a compensation is in particular also caused by the direct relationship between the tropospheric VCD and wind speed: an increase of the wind speed (divergence of the horizontal wind field) will in general be accompanied by a decrease of the tropospheric VCD. Thus the magnitude of the fluctuation of the wind field (e.g. expressed as standard deviation of wind data over a period of time) provides an upper bound for the related uncertainties of the emission estimate.

In addition to fluctuations of the wind field, also systematic changes during the period of the measurements can become important, especially if measurements with high trace gas VCDs are accompanied by strong deviations of the actual wind speed (or direction) from the assumed average values. This is e.g. the case if high trace gas VCDs are only measured at the beginning or end of a measurement loop, while the wind speed (or direction) systematically change during the period of the measurement. It is interesting to note here that in such cases the influence of any systematic offset in the measured tropospheric VCD (e.g. for zenith sky observations) can lead to additional uncertainties of the emission estimate.

Besides observational data (e.g. measured at meteorological stations at the ground) also results from model simulations can be used for the calculation of the trace gas flux and the uncertainties related to variations or imperfect knowledge of the wind field. Model data (as e.g. used by Johansson et al., 2008) have the advantage to yield information on the complete time-dependent 3-D distribution of the wind field over the encircled area. Thus in principle they allow the explicit consideration of the actual wind field at each measurement location. However, model data are not always available, especially at the appropriate spatial and temporal resolution (even the spatial resolution of regional models with grid sizes down to the kilometre scale might not always be sufficient). An alternative source of information is wind data from meteorological observations close to the locations of the car-MAX-DOAS observations. Such observations are often available from permanent measurement stations. Potential disadvantages are that meteorological data are not available for the individual measurement locations, and might only cover a part of the measurement area. In such cases they will not be fully representative for the average wind conditions across the encircle area. However, from ground based observations, fluctuations and systematic variations of the wind field can well be quantified, which yields important information for the error estimation.

Also, from meteorological observations usually no information on the vertical wind profile is available (exceptions are e.g. pilot balloons or radio sondes, see e.g. Rivera et al., 2009). Thus if only surface wind data are used, the effective wind speed relevant for the  $\text{NO}_2$  layer is probably underestimated. According to Eq. (2) this directly leads to an underestimation of the determined  $\text{NO}_2$  emissions. However, since most emission sources are located at the surface, it can be assumed that most of the freshly emitted  $\text{NO}_x$  should be also present close to the surface (exceptions are e.g. power plants). Thus the resulting underestimation will usually be small (at least compared to other uncertainties). Moreover it should be taken into account that even if information on the vertical wind profile was available, the uncertainties could not necessarily be largely reduced, because the vertical trace gas profile is still unknown.

For the quantification of errors caused by imperfect knowledge and variability of the wind field, in this study we use wind data from three meteorological stations inside the encircled area. These data are given as half hour mean values of wind direction and wind speed, from which the mean values and standard deviations for the four individual loops are calculated (see Table 1). For each loop 12 half hour mean values (for 3 stations, and for the period of 2 h) are used. It should be noted that the standard deviations for spatial or temporal variations are similar. For the measured average wind speeds (2.2 to 3.2 m/s), a half hour interval corresponds to a distance of about 4 to 6 km, which is similar to the distances between the different meteorological stations. Thus the standard deviation of the selected half hour averages can be regarded

as representative for fluctuations of the wind field on scales of about 5 km. Since this distance is still smaller compared to the extension of the encircled area (and also compared to the areas with enhanced trace gas VCDs), the effects of fluctuations of the wind field can be expected to mainly cancel out. As a conservative estimate of the remaining errors we thus use half of the standard deviation determined from the 12 half-hour data of the three stations (see Table 2). Besides fluctuations of the wind field, also systematic temporal changes during the measurement period occurred. As discussed above, such systematic changes could in principle lead to large errors of the emission estimates. However, since for most of the loops high  $\text{NO}_2$  VCDs are measured both at the beginning and the end of the loops, the effects of systematic changes should mainly cancel out. Thus, (and because the systematic variations during the individual loops are usually small compared to the standard deviations) in this study we did not explicitly take the effect of systematic variations of the wind fields into account. Implicitly, however, it is partly considered by the averaging of the emissions obtained for the consecutive loops.

It is interesting to note here that especially for measurements with the average wind direction almost parallel to parts of the driving route (e.g. as in circle 2) the uncertainties caused by fluctuations of the wind direction become especially large (see Table 2). For most circles, the respective errors are rather small, typically in the range of 10%. However, for the second circle (with the average wind direction almost parallel to larger parts of the driving route) the error is  $>30\%$ .

## 4.2 Errors caused by chemical transformations

### 4.2.1 Estimation of the $\text{NO}_x$ lifetime

In this section the effect of the finite atmospheric lifetime of  $\text{NO}_x$  (factor  $c_\tau$  in Eq. (4) is estimated. The  $\text{NO}_x$  lifetime depends on meteorological parameters (e.g. temperature) and on the photochemical state of the atmosphere, and is difficult to determine for the specific situation of our measurements. Thus we use an average value of 6 h for the  $\text{NO}_x$  lifetime which is derived from several experimental studies (Beirle et al., 2003, 2004a,b). According to the extension of the circles and the average wind speeds (Table 1) the time for the air masses to cross the encircled area is about 2 h. Assuming most  $\text{NO}_x$  is emitted close to the center of the encircled area, the effective transport time would be 1 h. Within that duration the  $\text{NO}_x$  concentration decreases by about 15% for an assumed lifetime of 6 h. This results in a correction factor  $c_\tau$  of 1.18. For assumed lifetimes of 4 and 8 hours the correction factors would be 1.28 and 1.13, respectively. From this variation we estimate the uncertainty caused by the finite atmospheric lifetime of  $\text{NO}_x$  to about 10%.

**Table 3.** NO<sub>x</sub> emissions from the encircled area after corrections for the lifetime and NO<sub>x</sub> partitioning. The total error includes the sun of all error contributions (retrieval of the tropospheric VCD, wind field, NO<sub>x</sub> lifetime, NO<sub>x</sub> partitioning).

| Circle | time        | Influx<br>(molec./sec) | Outflux<br>(molec./sec) | NO <sub>x</sub> Emissions<br>(molecules/sec) | Total error |
|--------|-------------|------------------------|-------------------------|--|-------------|
| 1      | 10:30–12:00 | $-6.68 \times 10^{24}$ | $13.72 \times 10^{24}$  | $7.04 \times 10^{24}$                        | 32%         |
| 2      | 11:30–13:00 | $-5.49 \times 10^{24}$ | $10.35 \times 10^{24}$  | $4.86 \times 10^{24}$                        | 45%         |
| 3*     | 12:30–14:00 | $-4.50 \times 10^{24}$ | $10.96 \times 10^{24}$  | $6.46 \times 10^{24}$                        | 25%         |
| 4      | 13:30–15:00 | $-5.50 \times 10^{24}$ | $14.72 \times 10^{24}$  | $9.22 \times 10^{24}$                        | 25%         |

\*partly overlaps with L4

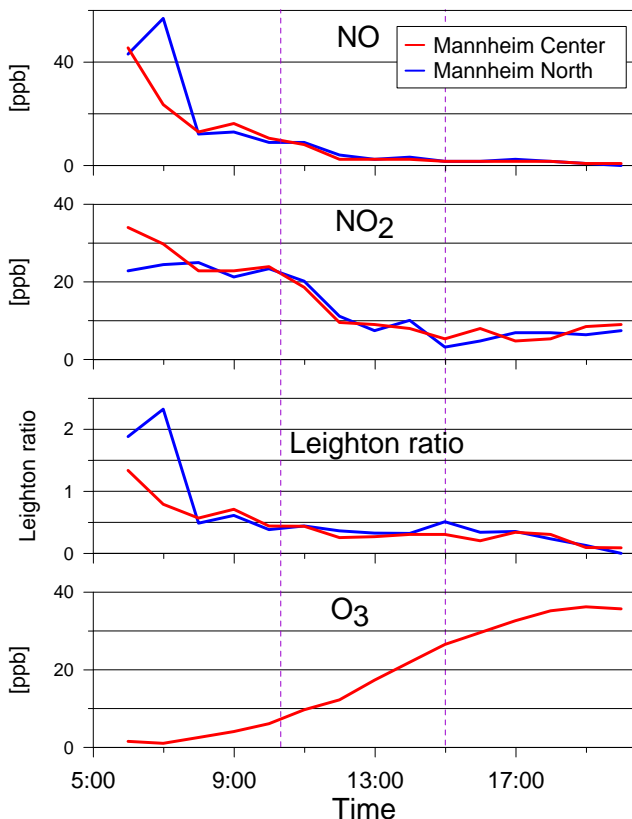


**Fig. 7.** Diurnal variation of the mixing ratios of NO, NO<sub>2</sub>, and O<sub>3</sub> for the stations Mannheim North and Mannheim center on 24 August 2006. Also the Leighton ratio is shown. The dashed vertical lines indicate the start and end times of the car MAX-DOAS measurements.

#### 4.2.2 Leighton ratio during the measurements

For the determination of the second correction factor  $c_L$  we use measurements of NO and NO<sub>2</sub> made at two meteorological stations (Mannheim North and Mannheim Center, see Fig. 7). For the period of the MAX-DOAS measurements Leighton ratios of about 0.35 were found. Thus we use a

correction factor  $c_L$  of 1.35 to determine the total NO<sub>x</sub> emissions. From the variation of the Leighton ratio during the time of our measurements we estimate the related uncertainties of the total emission to be about 10%.

#### 4.3 Final results of NO<sub>x</sub> emissions for the different circles

Table 3 summarises the total emissions and respective errors for the four circles. Also the absolute fluxes into or from the encircled area are shown. The calculated errors include the contributions associated with variations and imperfect knowledge of the wind field, NO<sub>x</sub> lifetime, NO<sub>x</sub> partitioning and retrieval of the tropospheric VCD.

The average of total NO<sub>x</sub> emission calculated from the results of the four circles (weighted by the respective errors) is  $(7.4 \pm 1.8) \times 10^{24}$  molecules/sec. This equals a NO<sub>x</sub> emission of 0.55 kg per second (the mass is calculated assuming that all NO<sub>x</sub> was NO<sub>2</sub>). The influges show a smaller variability ( $5.4 \pm 0.9 \times 10^{24}$  molec/sec) indicating that the variations of the outflux ( $12.8 \pm 1.8 \times 10^{24}$  molec/sec) are indeed caused by variations of the encircled emissions.

#### 4.4 Effect of ozone depletion

In some cases, additional complications can occur, e.g. if the NO concentrations are higher than the background ozone concentrations. Such situations might occur close to the stacks of power plants. Then the reaction of NO with ozone will eventually consume all available ozone, which prevents the further conversion of NO into NO<sub>2</sub>. Only after additional ozone-rich air is mixed with the ozone-depleted air masses, the Leighton ratio expected for ozone-rich conditions can be established. For our measurements the ozone mixing ratio measured at the different stations (see Fig. 7) is found to be higher than the NO<sub>x</sub> concentration for most of the time (after 11:00). However, especially for emissions from the large power plant in the southern part of Mannheim these conditions might not be fulfilled and the measured NO<sub>2</sub> might underestimate the total NO<sub>x</sub> emissions. Unfortunately, with our current knowledge this effect can not be quantified. Since the ozone concentrations increase during the day (Fig. 7),

the possible underestimation should be smaller for the later measurements. The effect of suppressed NO to NO<sub>2</sub> conversion should be investigated in more detail in future studies.

## 5 Conclusions

We applied car MAX-DOAS observations for the determination of the total NO<sub>x</sub> emissions from the Mannheim/Ludwigshafen industrial and urban area. This method is similar to that introduced by Johansson et al. (2008), but instead of measuring scattered sun light from zenith sky observations, we measure under a different angles with a MAX-DOAS instrument mounted on a car. MAX-DOAS observations measure scattered sunlight under various slant elevation angles and thus provide increased sensitivity and reduced uncertainties for tropospheric species. Moreover, MAX-DOAS observations allow to determine the absolute value of the vertically integrated tropospheric trace gas concentration (tropospheric VCD). Observations of the tropospheric VCD without systematic offsets are important if the measurements are not performed on closed loops, but only along selected transects through the emission plume. In such cases car MAX-DOAS observations allow to quantify the absolute value of the total trace gas flux, which can e.g. be directly compared to model simulations. Knowledge of the absolute tropospheric VCDs can become also important for closed-loop measurements if the effects of systematically varying wind fields or chemical transformations have to be considered (for example for circles around extended emissions sources).

Car MAX-DOAS observations (like zenith sky observations) provide a rather simple and cheap method for the determination of total emissions of extended areas like complete cities. Thus they allow to check existing emission estimates with a completely independent method. As shown by Johansson et al. (2008) besides NO<sub>2</sub> also the emissions of other species like e.g. SO<sub>2</sub> and HCHO can be quantified. In most cases the main uncertainties of the method are caused by temporal and spatial variations of the wind field across the encircled area. Additional errors are related to chemical transformations between the emission source and the location of the measurement. In this study we quantified the respective errors from in-situ observations within the encircled area.

On 24 August 2006 we performed Car MAX-DOAS observations on 4 consecutive circles around the cities of Mannheim and Ludwigshafen. The determined total emissions for these 4 circles range from  $4.9 \times 10^{24}$  to  $9.2 \times 10^{24}$  molec/sec with an average value of  $(7.4 \pm 1.8) \times 10^{24}$  molec/s. If simply extrapolated to a complete year a value of  $17\,830 \pm 4340$  tons NO<sub>x</sub>/per year (the mass is calculated assuming that all NO<sub>x</sub> was NO<sub>2</sub>) is derived, which compares well with existing emission estimates of both cities. For Ludwigshafen NO<sub>x</sub> emissions of 7950 tons

per year are reported for 2004 (Landesamt für Umwelt, 2008) and for Mannheim NO<sub>x</sub> emissions of 10121 tons per year are reported for 2002 (again assuming that all NO<sub>x</sub> was NO<sub>2</sub>) (Regierungspräsidium Karlsruhe, 2006). Both values sum up to 18071 tons per year. The average influx into the Mannheim/Ludwigshafen area determined from our observations is  $(5.4 \pm 0.9) \times 10^{24}$  molec/sec (or  $13\,010 \pm 2170$  t/yr) and the average outflux  $(12.8 \pm 1.8) \times 10^{24}$  molec/sec (or  $13\,010 \pm 4340$  t/yr).

Emission estimates from car MAX-DOAS (or zenith sky) observations should be further improved, and especially the following aspects should be considered:

- The accuracy of the determination of the tropospheric VCD should be improved by the use of tropospheric air mass factors derived from radiative transfer simulations (instead of using simple geometric approximations). Especially for zenith sky observations multiple scattering effects can lead to large deviations (overestimations) of the geometric approximation compared to the true tropospheric air mass factor. For MAX-DOAS observations, the correct consideration of the relative azimuth angle between the viewing direction and the sun is especially important.
- More accurate wind data are needed, preferably for the exact times and locations of the measurements. For that purpose model simulations might be most useful. Another interesting option would be to measure the wind direction and speed directly on the car roof.
- For the determination of the effective wind speed relevant for the layer of the observed trace gas, more accurate information on the vertical trace gas profile is needed. Such information might be derived from regional model simulations. Alternatively, also simple transport calculations based on the atmospheric stability and turbulence might be used. Here it is important to note that in many cases the height of the boundary layer might not be a good estimate for the vertical extension of freshly emitted pollutants, because the vertical transport between the emission source and the location of the measurement might be too slow to fill the entire boundary layer close to the emission source.
- Clouds do not only affect the atmospheric absorption path lengths (see e.g. Johansson et al. (2008)) but also the partitioning of photochemical reactive species like e.g. NO/NO<sub>2</sub>. Thus more detailed knowledge on cloud properties can improve the emission estimates. For example, besides the O<sub>4</sub> absorptions (see Johansson et al., 2008), also the radiance measured by the DOAS instrument might be used.
- Also more detailed information on chemical species concentrations (e.g. O<sub>3</sub>) would be helpful to characterise and quantify chemical transformations and

partitioning. Such information might be derived from model simulations of regional chemistry and transport, but also from air pollution networks.

Finally, car MAX-DOAS observations should routinely be applied cover temporal variations of emissions on various time scales (from diurnal to seasonal variations).

*Acknowledgements.* For the interpretation of our measurements we used information on meteorology and chemical composition from three in-situ monitoring stations of the city of Mannheim (<http://mnz.lubw.baden-wuerttemberg.de/messwerte/aktuell>). We thank two anonymous reviewers for their very helpful comments.

The service charges for this open access publication have been covered by the Max Planck Society.

Edited by: H. Worden

## References

- Beirle, S., Platt, U., Wenig, M., and Wagner, T.: Weekly cycle of NO<sub>2</sub> by GOME measurements: a signature of anthropogenic sources, *Atmos. Chem. Phys.*, 3, 2225–2232, doi:10.5194/acp-3-2225-2003, 2003.
- Beirle, S., Platt, U., von Glasow, R., Wenig, M., and Wagner, T.: Estimate of nitrogen oxide emissions from shipping by satellite remote sensing, *Geophys. Res. Lett.*, 31, L18102, doi:10.1029/2004GL020312, 2004a.
- Beirle, S., Platt, U., Wenig, M., and Wagner, T.: Highly resolved global distribution of tropospheric NO<sub>2</sub> using GOME narrow swath mode data, *Atmos. Chem. Phys.*, 4, 1913–1924, doi:10.5194/acp-4-1913-2004, 2004.
- Bobrowski, N., Hönninger, G., Galle, B., and Platt, U.: Detection of bromine monoxide in a volcanic plume, *Nature*, 423, 273–276, 2003.
- Brinksma, E. J. G., Pinardi, R., Braak, H., Volten, A., Richter, A., Schönhardt, M., van Roozendaal, C., Fayt, C., Hermans, R. J., Dirksen, T., Vlemmix, A. J. C., Berkhout, D. P. J., Swart, H., Ötjen, F., Wittrock, T., Wagner, O. W., Ibrahim, G., de Leeuw, M., Moerman, R. L., Curier, E. A., Celarier, W. H., Knap, J. P., Veefkind, H. J., Eskes, M., Allaart, R., Rothe, A., Peters, J. M., and Levelt, P. F.: The 2005 and 2006 DANDELIONS NO<sub>2</sub> and Aerosol Validation Campaigns, *J. Geophys. Res.*, 113, D16S46, doi:10.1029/2007JD008808, 2008.
- Bogumil, K., Orphal, J., Homann, T., Voigt, S., Spietz, P., Fleischmann, O. C., Vogel, A., Hartmann, M., Bovensmann, H., Frerik, J., and Burrows, J. P.: Measurements of Molecular Absorption Spectra with the SCIAMACHY Pre-Flight Model: Instrument Characterization and Reference Data for Atmospheric Remote-Sensing in the 230–2380 nm Region, *J. Photochem. Photobiol. A.*, 157, 167–184, 2003.
- Deutschmann, T. and Wagner, T.: TRACY-II Users manual, (<http://joseba.mpch-mainz.mpg.de/Strahlungstransport.htm>), 2008.
- Fayt, C. and Van Roozendaal, M.: WinDOAS 2.1 Software User Manual, (<http://www.oma.be/BIRA-IASB/Molecules/BrO/WinDOAS-SUM-210b.pdf>), 2001.
- Greenblatt G. D., Orlando, J. J., Burkholder, J. B., and Ravishankara, A. R.: Absorption measurements of oxygen between 330 and 1140 nm, *J. Geophys. Res.*, 95, 18577–18582, 1990.
- Hönninger G. and Platt U.: Observations of BrO and its vertical distribution during surface ozone depletion at Alert, *Atmos. Environ.*, 36, 2481–2490, 2002.
- Johansson, M., Galle, B., Yu, T., Tang, L., Chen, D., Li, H., Li, J. X., and Zhang, Y.: Quantification of total emission of air pollutants from Beijing using mobile mini-DOAS, *Atmos. Environ.*, 42, 6926–6933, 2008.
- Johansson, M., Rivera, C., de Foy, B., Lei, W., Song, J., Zhang, Y., Galle, B., and Molina, L.: Mobile mini-DOAS measurement of the outflow of NO<sub>2</sub> and HCHO from Mexico City, *Atmos. Chem. Phys.*, 9, 5647–5653, doi:10.5194/acp-9-5647-2009, 2009.
- Kraus, DOASIS, A Framework Design for DOAS, PhD-thesis, University of Mannheim ([http://hci.iwr.uni-heidelberg.de/publications/dip/2006/Kraus\\_PhD2006.pdf](http://hci.iwr.uni-heidelberg.de/publications/dip/2006/Kraus_PhD2006.pdf)), 2006.
- Kurucz, R. L., Furenid, I., Brault, J., and Testerman, L.: Solar flux atlas from 296 nm to 1300 nm, National Solar Observatory Atlas No. 1, Office of University publisher, Harvard University, Cambridge, 1984.
- Landesamt für Umwelt, Luftreinhalte- und Aktionsplan Ludwigshafen, Fortschreibung 2007–2015, (<http://www.luwg.rlp.de/icc/luwg/nav/d20/binarywriterservlet?imgUId=d5a5ebba-f225-911a-3b21-7128749cab66&uBasVariant=11111111-1111-1111-1111-111111111111&isDownload=true>), published by Landesamt für Umwelt, Wasserwirtschaft und Gewerbeaufsicht, Mainz, Germany, October 2008.
- Platt, U., and Stutz, J., *Differential Optical Absorption Spectroscopy, Principles and Applications*, Springer, Berlin, 2008.
- Regierungspräsidium Karlsruhe, Luftreinhalte-/Aktionsplan für den Regierungsbezirk Karlsruhe, Teilplan Mannheim (<http://www.mannheim.de/io2/download/webseiten/politik/aemter/fb63/dokumente/luftreinhalteplan.pdf>), published by Regierungspräsidium Karlsruhe, Germany, March 2006.
- Rivera, C., Sosa, G., Whrnshimmel, H., de Foy, B., Johansson, M., and Galle, B.: Tula industrial complex (Mexico) emissions of SO<sub>2</sub> and NO<sub>2</sub> during the MCMA 2006 field campaign using a mobile mini-DOAS system, *Atmos. Chem. Phys.*, 9, 6351–6361, doi:10.5194/acp-9-6351-2009, 2009.
- Rothman, L. S., Jacquemart, D., Barbe, A., Benner, D. C., Birk, M., Brown, L. R., Carleer, M. R., Chackerian Jr., C., Chance, K., Coudert, L. H., Dana, V., Devi, V. M., Flaud, J.-M., Gamache, R. R., Goldman, A., Hartmann, J.-M., Jucks, K. W., Maki, A. G., Mandin, J.-Y., Massie, S. T., Orphal, J., Perrin, A., Rinsland, C. P., Smith, M. A. H., Tennyson, J., Tolchenov, R. N., Toth, R. A., Vander Auwera, J., Varanasi, P., and Wagner, G.: The HITRAN 2004 molecular spectroscopic database, *J. Quant. Spectrosc. Ra.*, 96, 139–204, 2005.
- Theys, N., Van Roozendaal, M., Hendrick, F., Fayt, C., Hermans, C., Baray, J.-L., Goutail, F., Pommereau, J.-P., and De Mazière, M.: Retrieval of stratospheric and tropospheric BrO columns from multi-axis DOAS measurements at Reunion Island (21° S, 56° E), *Atmos. Chem. Phys.*, 7, 4733–4749, doi:10.5194/acp-7-4733-2007, 2007.
- Vandaele, A. C., Hermans, C., Simon, P. C., Carleer, M., Colin, R., Fally, S., Mérienne, M.-F., Jenouvrier, A., and Coquart, B.: Measurements of the NO<sub>2</sub> Absorption Cross-section from 42 000 cm-

- 1 to 10000 cm<sup>-1</sup> (238–1000 nm) at 220 K and 294 K, *J. Quant. Spectrosc. Radiat. Transfer*, 59, 171–184, 1997.
- Van Roozendael, M., Fayt, C., Post, P., Hermans, C., Lambert, J.-C.: Retrieval of BrO and NO<sub>2</sub> from UV-Visible Observations, in: *Sounding the troposphere from space: a new era for atmospheric chemistry*, edited by: Borrell, P. M., Burrows, J. P., Platt, U., et al., Springer, Heidelberg, ISBN 3-540-40873-8, 2003.
- Wagner, T., Dix, B., Friedeburg, C. v., Frieß, U., Sanghavi, S., Sinreich, R., and Platt, U.: MAX-DOAS O<sub>4</sub> measurements – a new technique to derive information on atmospheric aerosols. (I) Principles and information content, *J. Geophys. Res.*, 109, D22205, doi: 10.1029/2004JD004904, 2004.
- Wagner, T., Burrows, J. P., Deutschmann, T., Dix, B., von Friedeburg, C., Frie, U., Hendrick, F., Heue, K.-P., Irie, H., Iwabuchi, H., Kanaya, Y., Keller, J., McLinden, C. A., Oetjen, H., Palazzi, E., Petritoli, A., Platt, U., Postlyakov, O., Pukite, J., Richter, A., van Roozendael, M., Rozanov, A., Rozanov, V., Sinreich, R., Sanghavi, S., and Wittrock, F.: Comparison of box-air-mass-factors and radiances for Multiple-Axis Differential Optical Absorption Spectroscopy (MAX-DOAS) geometries calculated from different UV/visible radiative transfer models, *Atmos. Chem. Phys.*, 7, 1809–1833, doi:10.5194/acp-7-1809-2007, 2007.
- T. Wagner, O. Ibrahim, R. Shaiganfar, and U. Platt: Mobile MAX-DOAS observations of tropospheric trace gases *Atmos. Meas. Tech.*, 3, 129–140, 2010.
- Wittrock, F., Oetjen, H., Richter, A., Fietkau, S., Medeke, T., Rozanov, A., and Burrows, J. P.: MAX-DOAS measurements of atmospheric trace gases in Ny-Ålesund Radiative transfer studies and their application, *Atmos. Chem. Phys.*, 4, 955–966, doi:10.5194/acp-4-955-2004, 2004.